Sustainable Food Technology

Accepted Manuscript

This article can be cited before page numbers have been issued, to do this please use: X. Zhang, T. Xiao, D. J. McClements, H. Hu, J. Zhu, X. Ma, Q. Wang and A. Shi, *Sustainable Food Technol.*, 2026, DOI: 10.1039/D6FB00023A.

ROYAL SOCIETY OF CHEMISTRY

View Article Online
DOI: 10.1039/D6FB00023A

This study optimizes foaming properties of soybean/mung bean proteins via pH-regulated hot-pressing. As sustainable alternatives to animal proteins, enhanced plant proteins promote high-value resource utilization, expand food industry applications, and support eco-friendly production, advancing food system sustainability.

View Article Online
DOI: 10.1039/D6FB00023A

ARTICLE

The Effect of Heat and Pressure Treatment at Different pH Levels on the Foaming Properties and Surface Properties of Soy Protein Isolate and Mung Bean Protein

Received 00th January 20xx,
Accepted 00th January 20xx

DOI: 10.1039/x0xx00000x

*Xinyu Zhang [a 1], Tianlong Xiao [a, b 1], David Julian McClements [c], Hui Hu [a], Jinjin Zhu [a], Xiaojie Ma [a] *, Qiang Wang [a, b] *, Aimin Shi [a, b] **

Abstract: Plant proteins are widely used in food systems due to their sustainability, but their relatively poor foaming properties limit broader applications. This study explored the effect of hot-pressing soybean and mung bean proteins at different pH values on their structural, interfacial, and foaming properties. Hot-pressing enhanced the protein foaming capacity at all pH values without affecting stability. At pH 5, isoelectric precipitation caused protein aggregation and increased the particle size, turbidity, and sedimentation. This led to less efficient protein adsorption on the air-bubble surfaces and a lower foaming capacity. Spectroscopy showed that proteins were more flexible under alkaline conditions, reducing the air - water surface tension and increasing the foaming capacity. Optimizing the treatment pH allows hot pressing to improve the foaming properties of plant proteins, thereby expanding their application in the food industry.

1 Introduction

Foam provides ideal texture and sensory characteristics for a variety of foods, including whipped cream, egg whites, coffee, beer, ice cream, and marshmallows[1]. Egg white protein is widely used as a foaming agent because of its excellent functional properties and high nutritional value. However, compared with traditional animal protein foods, plant protein foods are receiving more attention from consumers worldwide because of their health benefits and environmental friendliness. Enhancing the functionality of plant proteins also facilitates their incorporation into protein-rich foods targeted at vulnerable groups, such as the elderly. This would broaden the significance of this research. A recent study by Wang et al. examined how factors associated with ageing alter protein requirements, highlighting the importance of developing palatable, foam-based plant protein foods for elderly consumers[2]. Among the many plant proteins, soy protein isolate (SPI) has become one of the most widely used commercial plant proteins due to its excellent functional characteristics, rich nutritional value and low cost[3]. SPI is a protein mixture primarily composed of glycinin and β-conglycinin, with molecular weights of approximately 360 kDa and 180 kDa, respectively, which exhibit distinct properties at the air-water interface[4]. Structurally, soy globulin (hexamer) and β-companion soy globulin (trimer) in SPI possess high surface hydrophobicity and moderate solubility; their flexible molecular conformation enables them to adsorb rapidly onto the gas–water interface, unfold, and form a dense, elastic interfacial film, thereby conferring excellent foaming capacity and good foam stability on SPI[5]. In contrast, mung bean protein (MBP), which consists primarily of 8S globulins, has a more flexible and loosely structured nature, facilitating rapid diffusion and adsorption at the gas–water interface. This structural characteristic typically results in stronger foaming capacity but weaker interfacial film strength. Consequently, MBP generally exhibits good foaming capacity but relatively poor foam stability[6]. The differences between SPI and MBP in terms of molecular structure, flexibility, and interfacial behavior highlight their distinct roles in foam formation and stabilization processes, providing important insights into their potential synergistic applications in food systems.

Generally, the functional characteristics of proteins are key factors in determining their potential for widespread application in the food industry. For example, the interfacial properties of proteins directly determine their suitability as emulsifiers or foaming agents. However, most plant proteins have relatively weak adsorption capacities at the air-water interface due to their relatively dense structures. Therefore, modifying the structure of plant proteins (such as SPI and MBP) to enhance their foaming properties is of great significance for expanding their applications in the food industry.

A large body of research has reported on the modification of the secondary and tertiary structures of plant proteins to improve their foaming properties and surface activity, thereby expanding their applications in food production. Methods such as heat treatment, ultrasonication, pressure treatment, and enzymatic hydrolysis have been employed to induce specific conformational changes to achieve desirable surface properties.[7] Heat treatment is an economical,

[a] Institute of Food Science and Technology, Chinese Academy of Agricultural Sciences, Comprehensive Utilization Laboratory of Cereal and Oil Processing, Ministry of Agriculture and Rural, Beijing 100193, China.
[b] College of Light Industry and Food Sciences, Zhongkai University of Agriculture and Engineering, Guangzhou 510225, China.
[c] Department of Food Science, University of Massachusetts Amherst, Amherst, MA 01003, USA.
*Corresponding authors
Aimin Shi, E-mail: shiaimin@caas.cn,
Qiang Wang, E-mail: wangqiang06@caas.cn
Xiaojie Ma, E-mail: maxiaojie@caas.cn

efficient, environmentally friendly, and convenient physical processing method. This method disrupts hydrogen and disulfide bonds, causing the amino acid chains to denature and unfold, thereby forming protein aggregates and significantly altering the functional properties of the protein. This process may significantly affect the interfacial behavior of the protein[8]. Heat treatment also alters the tertiary structure of WPI, improving its emulsifying and foaming properties. Liu et al. reported that heat treatment altered the secondary and tertiary structures of the winged bean isolate; when heated at 75°C for 45 min, the emulsifying and foaming properties reached their peak, with the foaming capacity increasing from 11.67% to 47.50%[9]. High-pressure homogenization (HPH) is a promising technique for effectively improving the functional properties of plant proteins. During homogenization, high-intensity mechanical shear forces and turbulent flow disrupt the hydrophobic interactions that maintain protein aggregates. This not only reduces the particle size of the protein but also induces moderate denaturation of the protein molecular structure, exposing active functional groups that were previously buried within the molecule, thereby significantly optimizing the protein's functional properties[10]. For example, Yan et al. significantly improved the foaming capacity of pea protein isolates through high-pressure homogenization[11].

pH adjustment is an efficient chemical method that can be used to alter the functional properties of proteins. When proteins are placed under extreme acidic or alkaline conditions, that is, far from their isoelectric point, the electrostatic repulsion between molecules increases, causing the proteins to partially unfold. Subsequently, when the pH is adjusted back to neutral (pH 7), the protein refolds into a more flexible conformation, referred to as the 'melted state'[12] This unfolding and refolding process significantly impacts the protein's structural and functional properties. For example, Othmeni et al. found that under neutral pH conditions, foam volume stability reaches its peak. At pH 5, larger protein aggregates near the isoelectric point may help form thicker and more viscous interfacial films, resulting in smaller and more uniform bubbles and enhanced bubble retention capacity[13]. Ma et al. demonstrated that lupin protein (LP) exhibited high foam overflow rates of 300% and 331% at pH values of 4 and 3.5, respectively. This indicates that lupin protein exhibits excellent foaming properties under acidic conditions[14]. Although plant protein modification methods are usually applied individually, in recent years, an increasing number of studies have begun to focus on the synergistic effects of combining multiple treatment methods[15]. The combination of pH adjustment and physical processing can significantly enhance the functional properties of proteins. When subjected to heat treatment under alkaline conditions, protein molecules are prone to extensive and irreversible structural changes. When the pH of the protein is subsequently adjusted back to neutral, protein refolding is reduced. Studies have shown that this combination treatment can improve the solubility, emulsifiability, foaming properties, and gelling ability of various plant proteins, Including rice protein isolate[16], pea protein isolate[17], peanut protein isolate[18] and hemp seed protein[19] among others. However, there is limited research on improving the foaming properties of plant proteins through hot-pressing at different pH values.

Consequently, this study investigated the effects of thermal compression treatment on the structural and functional properties of SPI and MBP at different pH levels. Particular attention was paid to the impact of this treatment on the interfacial and foaming characteristics of these proteins. These findings support the use of plant proteins as functional ingredients in the food industry, particularly in the production of foods requiring a foamed structure, such as cakes, bread, ice cream, and mousses.

2.Materials and methods

2.1 Materials

Soybean protein isolate (SPI, 90% purity) was supplied by DuPont (Shanghai, China). Mung bean protein (MBP, 86% purity) was provided by Zhuoyuan Voyage Technology Development Co., ltd. (Beijing, China). 1-8-Anilino naphthalenesulfonate (ANS) was supplied by Cayman Chemical Company (Ann Arbor, MI, USA). Fluorescein isothiocyanate (FITC) was supplied by the Yuanye Bio-Technology Company (Shanghai, China). Distilled water was used to prepare all solutions.

2.2 Heat and pressure treatment of proteins under different pH conditions

Powdered SPI or MBP was dispersed in deionized water to a concentration of 6% (w/w) and then stirred for 2 h at room temperature. These protein dispersions were then stored overnight at 4℃ to allow complete hydration of the protein molecules. The pH of the protein solutions was then adjusted to 3, 5, 7, 9, or 11 using 4 mol/L hydrochloric acid or sodium hydroxide solution. Protein samples were then heated in an autoclave at 130℃ for 30 min. Then, they were immediately cooled in an ice bath and passed through a homogenizer three times at 500 bar. The samples were designated as SPI-0 (untreated) and MBP-0 (untreated); SPI-3, SPI-5, SPI-7, SPI-9, SPI-11, MBP-3, MBP-5, MBP-7, SPI-9, and SPI-11 correspond to the respective pH values.

2.3 Circular dichroism (CD) spectroscopy

Circular dichroism (CD) spectroscopy (JAS.C.O J-1500 spectrometer) was used to assess the secondary structure of the proteins. The samples were diluted to a concentration of 1 mg/mL protein. The following operating parameters were used: cuvette pathlength of 1 mm; scanning wavelength range of 190 to 250 nm; scanning rate of 60 nm/min; bandwidth of 1 nm[20].

2.4 Intrinsic fluorescence spectroscopy

The protein solution to be tested was diluted to a concentration of 0.25 mg/mL protein. The fluorescence spectra of the protein solutions were then determined using a fluorescence spectrophotometer (F-2500, Hitachi, Japan). The following operating parameters were used: excitation wavelength of 290 nm; scanning wavelength range of 300 to 500 nm; slit width of 5 nm; scanning speed of 200 nm/min; scanning interval of 20 ms, and reaction time of 0.1 s[21].

2.5 Particle size analysis

The particle size distribution of the protein was determined using a Zetasizer Nano ZS90 (Malvern Instruments Ltd., UK). The protein dispersion was diluted to a protein concentration of

0.1% (w/w). The temperature was set to 25 °C, with an equilibration time of 2 min[22].

2.6 Zeta potential

The surface charge of the particles in the protein dispersions was characterized using particle electrophoresis (Malvern Nano-ZS 90, Malvern Instruments Ltd., UK) at room temperature (25 ± 0.1°C). The protein dispersions were diluted to concentration of 0.1% w/w protein prior to analysis. The zeta-potentials were measured using the Smoluchowski model in the instrument software, with an F(ka) value of 1.5[23].

2.7 Turbiscan Stability Index (TSI)

The resistance of the protein dispersions to aggregation and sedimentation was characterized by measuring the transmission and backscattering of light as a function of sample height and time using a Turbiscan instrument (Turbisican Lab Tower, Germany). The protein solution was diluted to 1% (w/v) Initially, 20 mL samples were individually placed in specialized cylindrical sample glass vials. A pulsed near-infrared light source and two synchronized optical detectors were then used to measure the intensity of the transmitted light (T) and backscattered light (BS) from the sample with sample height. The optical detectors were scanned from the bottom to the top of the sample vials over the height range from 2 to 45 mm. Measurements were performed at 25 °C and the samples were scanned every 30 min for one day. The turbiscan stability index (TSI) was then calculated from the backscattering data using the following formula:

$$\mathbf{TSI} = \sum_{\mathbf{i}} \frac{\sum_{\mathbf{h}} |\mathbf{scan_i(h) - scan_{i-1}(h)}|}{\mathbf{H}} \quad (1)$$

Here, scani(h) is the average backscattered light index for each measurement (i), scani-1(h) is the average backscattered light index for the i-1st measurement, and h is the height of the sample.

2.8 Turbidity analysis

The turbidity of the samples was measured by measuring the amount of light that could pass through them. Initially, the protein dispersions were diluted to 1 mg/mL protein using deionized water and then the absorbance of the samples was measured at 600 nm using a UV-visible spectrophotometer (UV-2550, Shimadzu, Suzhou, China).

2.9 Surface hydrophobicity (H_0)

The protein dispersions were diluted with distilled water to obtain a range of different protein concentrations (0.05-0.5 mg/mL). Then, 0.024 g of ANS probe was dissolved in 10 mL of phosphate buffer solution (8 mM ANS). Afterward, 20 μ L of ANS solution was added to 4 mL of protein solution, and the mixture as shaken and then allowed to stand for 10 min. The fluorescence intensity was then measured on a fluorescence photometer (F-2500, Hitachi, Tokyo, Japan) using emission and excitation wavelengths of 470 nm and 390 nm, respectively. The measured fluorescence intensity was then plotted against the protein concentration, and the initial slope of the curve was designated as the surface hydrophobicity index (H_0) of the samples[24].

2.10 Surface tension

The protein dispersions were diluted to a protein concentration of 1% (w/w) using distilled water, and then vortexed for 1 min to mix them. The interfacial tension of the protein dispersions was then determined using an optical contact angle meter (OCA20, Stuttgart, Germany) at 25 ± 0.1 °C. Use the hanging drop method to drop 10 μL of water into the air. The densities of the air and sample were taken to be 1.185 kg/m^3 and 1001 kg/m^3, respectively, while the surface tension between a bare air-water interface was taken to be 72.0 ± 0.1 mN/m. Images of the samples were taken using a digital camera operating at a speed of 5 frames per second. The surface tension was then calculated form the shape of the droplets using the Young-Laplace equation[25].

2.11 Foaming capacity and foam stability

The foaming properties of the protein dispersions was determined by placing 10 mL of samples into a 50 mL measuring cylinder and then shearing at 10,000 r/min for 2 min[1]. The volume of the samples was then measured immediately after shearing (V1) and 15 min after shearing was completed (V2). The foaming capacity (FC) and foaming stability (FS) of the protein dispersions were then calculated as follows:

$$\boldsymbol{FC}\ (\%) = \frac{\boldsymbol{V_1 - 10}}{\mathbf{10}} \times \mathbf{100}\% \quad (2)$$

$$\boldsymbol{FS}\ (\%) = \frac{\boldsymbol{V_2 - 10}}{\boldsymbol{V_1 - 10}} \times \mathbf{100}\% \quad (3)$$

2.12 Foam density, overrun, and porosity

The density, overrun, and porosity of the foams were determined according to the method described by Dehghannya, with some changes[26]. Foams were prepared at room temperature according to the method described in Section 2.11 and then carefully poured into 15 mL vials and weighed. Care was taken to prevent disruption of the foam when they were transferred into the vials. The foam density, overrun, and porosity were then determined using the following formula:

$$\boldsymbol{\rho_f}\left(\mathbf{g \cdot cm^{-1}}\right) = \frac{\mathbf{W_f}}{\mathbf{15}} \quad (4)$$

$$\boldsymbol{Overrun}\ (\%) = \frac{\frac{\mathbf{1}}{\boldsymbol{\rho_f}} - \frac{\mathbf{1}}{\boldsymbol{\rho_l}}}{\frac{\mathbf{1}}{\boldsymbol{\rho_l}}} \times \mathbf{100}\% \quad (5)$$

$$\boldsymbol{Porosity}\ (\%) = \left(\mathbf{1} - \frac{\boldsymbol{\rho_f}}{\boldsymbol{\rho_l}}\right) \times \mathbf{100}\% = \left(\frac{\boldsymbol{Overrun \times 100}}{\boldsymbol{Overrun - 100}}\right) \quad (6)$$

Here, ρf is the density of the foam, ρl is the density of the original liquid (before foaming), and Wf is the weight of a known volume of the foam (15 mL).

2.13 Foam microstructure

The microstructure of the foams was assessed using confocal fluorescence microcopy. Initially, protein foams were prepared by blending aqueous protein dispersions using a high-speed shearing device at 10,000 r/min for 2 min. Then, 10 mL of foam sample was collected and 20 μL of FITC solution was added. A small amount of foam was then placed on a concave slide and observed using a confocal laser scanning microscope (CLSM) (TCS-SP8, Leica, Wetzlar, Germany). A 4× eyepiece lens and a 10× objective lens were used. Foam images were taken at different time intervals within the first 15 min.

2.14 Statistical analysis

View Article Online
DOI: 10.1039/D6FB00023J

All experiments were repeated three times, and the results expressed as mean ± standard deviation. The data were analyzed by ANOVA using IBM SPSS Statistics 26 software (IBM Inc.). Graph processing was performed using Origin 2022 software (OriginLab Corporation, Northampton, MA, USA).

3. Results and discussion

3.1 Circular dichroism (CD) spectroscopy

The natural structure of proteins is regulated by various physical interactions, including van der Waals forces, hydrogen bonds, ionic bonds, hydrophobic interactions, and entropy effects[27] When proteins are exposed to thermal energy, the relative importance of molecular interactions and entropy contributions within them changes. Consequently, globular proteins undergo conformational changes, which affect their secondary and tertiary structures[28]. The extent of these changes would be expected to depend on pH, as this impacts the ionization state of some amino acid side groups (such as amino and carboxyl groups), which will alter the attractive and repulsive electrostatic interactions within the polypeptide chain[29].

The secondary structure of proteins is a key determinant of their functions. In this study, circular dichroism (CD) spectroscopy was employed to determine the secondary structure proportions of SPI and MBP following heat and pressure treatment at different pH values (Figure 1). The results showed that in untreated SPI (SPI-0), the proportions of α-helix, β-sheet, β-turn, and random coil were 18.2%, 30.1%, 21.57%, and 30.1%, respectively; the corresponding proportions in untreated MBP (MBP-0) were 19.97%, 20.33%, 29.4%, and 30.33%, respectively. The secondary structures of both plant proteins exhibited highly consistent patterns in response to pH changes. Under acidic conditions (pH 3–5), the α-helix and β-turn contents decreased significantly, whereas the β-sheet content increased substantially. The proteins predominantly adopted aggregated structures formed by intermolecular rearrangement, which hindered uniform adsorption at the interface and was detrimental to the formation of a stable interfacial film. As the pH increased to weakly alkaline conditions (pH 9), the proportion of β-sheets decreased significantly, whereas the proportion of random coils reached a peak. This has also been confirmed as a key factor in enhancing foaming activity in the study by Othmeni et al. on legume proteins[13]. This indicates that the proteins undergo maximum denaturation and structural relaxation, allowing their internally buried hydrophobic groups to be fully exposed to the solvent. This conformational state not only reduces the gas–liquid interfacial tension but also accelerates the adsorption rate of proteins at the interface, laying the kinetic foundation for foam formation. Furthermore, the pH-mediated strong electrostatic repulsion effectively inhibits excessive protein aggregation, promoting the formation of a uniform, continuous, and highly viscoelastic protective film at the interface. This film prevents bubble coalescence through steric hindrance and electrostatic repulsion, thereby significantly enhancing the stability of the foam. However, under strongly alkaline conditions (pH 11), excessive denaturation of the proteins tends to induce irreversible aggregation, which weakens the mechanical toughness of the interfacial film, leading to a decline in foam stability.

3.2 Intrinsic fluorescence spectroscopy

The intrinsic fluorescence spectra of proteins further elucidate the influence of pH on the molecular conformation of plant proteins during thermal and pressure treatments. The intensity and wavelength of the intrinsic fluorescence signals generated by phenolic hydroxyl groups (such as tryptophan) in proteins are highly sensitive to the polarity of the surrounding environment. Consequently, the fluorescence quantum yield of tryptophan can be used to characterize changes in the tertiary structure of proteins[12]. This method can detect changes in protein conformation or aggregation states, which alter the local environment of the aforementioned groups [21]. Under different pH conditions, the intensity of the fluorescence peak in proteins subjected to thermal compression treatment increased significantly. This effect can be attributed to the thermal compression environment employed in the treatment, which promotes protein unfolding and disrupts protein aggregates. Certain tryptophan groups, originally located within the hydrophobic interior of the protein molecule or aggregate, are exposed to the surrounding water, which increases the polarity of their local environment and thereby enhances the fluorescence signal[30]. The foaming capacity, foam stability, and interfacial adsorption properties of proteins essentially depend on the flexibility of their molecular conformation, the degree of exposure of hydrophobic groups, and the strength of intermolecular forces; these characteristics can all be indirectly characterized through changes in the intrinsic fluorescence spectrum.

Based on the autofluorescence results, pH significantly influences the foaming and interfacial properties of proteins under thermal and pressure conditions by regulating their conformational state. With regard to these two proteins (Fig. 1CD), When the pH deviates from the protein's isoelectric point (approximately 5), particularly under strongly alkaline conditions (pH 9 and 11), fluorescence intensity reaches its peak, indicating that the protein molecules are most unfolded at this point. Hydrophobic groups (including tryptophan residues) that were originally buried within the molecule are extensively exposed. Simultaneously, the polypeptide chains carry a high negative charge due to the complete deprotonation of carboxyl groups (-COO^-), resulting in enhanced electrostatic repulsion between molecules. This effectively inhibits the aggregation of protein molecules, making them more readily dispersible in the aqueous phase.[31]. Our study found that changes in the pH of SPI and MBP increased fluorescence intensity, This is consistent with previously reported data [32]; [33]. This highly negatively charged state not only inhibits protein aggregation but also enhances the interaction between protein molecules and the aqueous phase, improving their dispersion in the aqueous phase and providing favorable conditions for their adsorption and foaming at the gas–liquid interface.

View Article Online
DOI: 10.1039/D6FB00023A

Conversely, near the protein isoelectric point (pH 5), the fluorescence intensity decreases significantly, which is closely related to reduced protein unfolding and increased molecular aggregation[34]. Near the isoelectric point, electrostatic repulsion between proteins weakens, making them more prone to aggregation, thereby further reducing the number of non-polar groups exposed to water. This aggregated state not only leads to a weakened fluorescence signal but also directly results in reduced protein surface activity, with a significant decrease in foaming capacity and foam stability, as aggregated protein molecules struggle to perform their core functions of interfacial adsorption and membrane formation.

Considering both foaming and interfacial properties, the high fluorescence intensity of the two plant proteins under strongly alkaline conditions corresponds to their fully unfolded molecular conformation and extensive exposure of hydrophobic groups. This conformational characteristic confers excellent interfacial activity, enabling rapid adsorption at the gas–liquid interface, effectively reducing interfacial tension, and forming stable foam structures. This is also consistent with the subsequent foaming results.

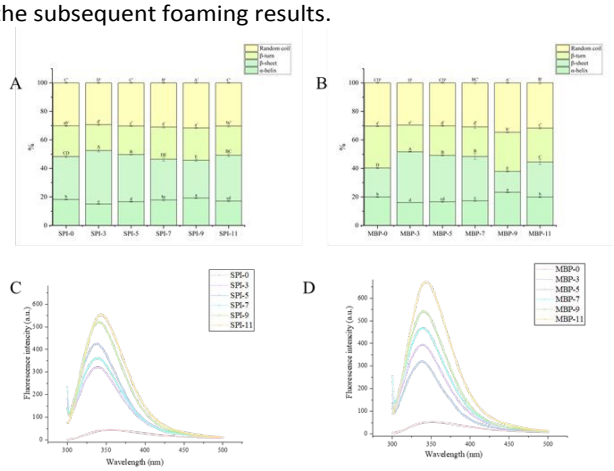

Figure 1 Effect of heat-pressing treatment at different pH values on the secondary structure (A, B) and intrinsic fluorescence (C, D) of soybean protein isolate (SPI) and mung bean protein (MBP). SPI-0 and MBP-0 denote untreated samples, whereas the numbers following SPI and MBP (3, 5, 7, 9, and 11) indicate the pH values of the treated samples. Different letters above the bar charts indicate significant differences between groups ($p < 0.05$)

3.3 Particle size analysis

The particle size of proteins significantly affects their surface activity (FA) because it influences their adsorption at the gas-liquid interface[35]. Particle size information for the two protein dispersions was obtained through light scattering analysis (Table 1). The untreated protein samples contained relatively large particles (>10 μm), indicating significant protein aggregation during separation and purification. Under different pH conditions, the particle sizes of SPI and MBP solutions significantly decreased after high-humidity heat treatment, indicating that the higher temperatures effectively disrupted the protein aggregates present in the raw materials[36].

Heat and pressure treatment carried out under different pH conditions significantly affected the particle size of the protein dispersion. For both plant proteins, the greatest aggregation was observed at pH 5, which can be attributed to the precipitation of protein molecules near their isoelectric point due to the weakening of electrostatic repulsive forces[37]. Conversely, the smallest protein aggregates were observed under highly alkaline conditions (pH 11), which can be attributed to the strong electrostatic repulsion between highly negatively charged protein molecules under these conditions[38]. This is consistent with the changes in the particle size of chickpea protein treated under different pH conditions[12]. Generally, smaller protein particles are preferred for foam preparation because they can easily adsorb to the gas-liquid interface during shear and form a protective coating around the bubbles[39]. Therefore, the significant reduction in particle size observed when proteins are subjected to high humidity and heat at specific pH values may be beneficial for their foaming performance.

3.4 Particle charge analysis

The surface potential of proteins also affects their foaming properties. Generally, a reduction in zeta potential facilitates protein adsorption at the gas-liquid interface by weakening the electrostatic barrier there[40]. The isoelectric points (pI) of SPI and MBP are approximately 4.5–5.0 and 4.2–4.6, respectively. By measuring the zeta potential values of plant protein particles (Table 1), insights were gained into how pH influences the electrical properties of these particles during high-humidity heat treatment. The solution's pH is anticipated to alter the pH of the protein particles by affecting the protonation and deprotonation of the amino and carboxyl groups on their surface[41].

The particles in SPI and MBP dispersions exhibited strong positive charges of 23.83 mV and 20.7 mV, respectively, under acidic conditions (pH 3), and strong negative charges of -35.43 mV and -33.1 mV, respectively, under alkaline conditions (pH 11), with their zero-charge points slightly below pH 5. At low pH values, protonated amino groups tend to carry a positive charge ($-NH_3^+$), whereas protonated carboxyl groups tend to be neutral ($-CO_2H$). Therefore, the net charge of proteins below the isoelectric point was positive. Conversely, at high pH values, deprotonated carboxyl groups tend to carry a negative charge ($-CO_2^-$), whereas deprotonated amino groups tend to be neutral ($-NH_2$). Therefore, the net charge of proteins above the isoelectric point was negative. This is consistent with the effect of pH changes on the zeta potential of pea protein isolates [13]. When the pH is in the acidic range, as the pH decreases and the hydrogen ion concentration in the solution increases, the negative charges on the protein molecule surface are neutralized, and the protein molecule may become positively charged, with the potential changing from negative to positive. When protein molecules aggregate, the potential decreases and approaches zero. At this point, the protein stability is the lowest, and it is prone to flocculation or precipitation[42]. Conversely, in an alkaline environment, protein molecules acquire more hydroxide ions, increasing the density of negative charges on their surfaces and the absolute value of the potential. As the pH value increases, the absolute value of the protein potential increases, and the stability of the protein improves[43].

View Article Online
DOI: 10.1039/D6FB00023A

ARTICLE

Table 1. Impact of pH on the mean particle diameter and zeta potential of soy protein isolate (SPI) and mung bean protein (MBP)samples.

pH	SPI		MBP	
	Z-Average (nm)	Zeta Potential (mV)	Z-Average (nm)	Zeta Potential (mV)
Untreated	36,770.0 ± 780^{a}	-28.2 ± 0.0^{D}	99200.0 ± 220^{a}	-15.4± 0.3^{D}
3	292.8 ± 1.3^{c}	23.8 ± 0.1^{A}	155.1 ±0.4^{cd}	20.7 ± 0.1^{A}
5	1691.3 ± 2.6^{b}	-5.9 ± 0.0^{B}	1953.7 ±4.1^{b}	-14.8 ± 0.1^{C}
7	280.2 ± 3.8^{d}	-22.1 ± 0.1^{C}	161.7 ±1.5^{c}	-10.2 ± 0.1^{B}
9	223.3 ± 1.0^{e}	-29.6 ± 0.0^{E}	112.67 ± 0.3^{de}	-28.2 ± 0.2^{E}
11	80.3 ± 1.0^{f}	-35.4 ± 0.4^{F}	77.80 ± 0.36^{e}	-33.1 ± 0.4^{F}

3.5 Turbiscan Stability Index (TSI) analysis

The Turbiscan Stability Index (TSI) value of protein dispersions reflects their ability to resist aggregation and sedimentation; the lower the value, the higher the stability[44]. The changes in TSI values over a 24-hour period were recorded for protein dispersions subjected to heat-pressure treatment at different pH levels (Figures 2A and 2B). For SPI and MBP dispersions, the fastest and largest increases in TSI values occurred at pH 5 during storage. This phenomenon can be attributed to the presence of relatively large and dense protein particles that rapidly migrate downward under the gravitational force. This is consistent with the particle size results obtained. Other samples exhibited lower sedimentation rates and degrees, possibly owing to their smaller particles and the formation of loosely aggregated particle networks, which exhibit greater resistance to separation.

3.6 Turbidity

The turbidity of colloidal dispersions is sensitive to the size of the particles within them; therefore, turbidity measurements can be used to reveal information about protein aggregation[45]. However, it should be noted that there is no simple linear relationship between the particle size and turbidity. As the particle size increases, the turbidity first increases until it reaches a maximum value (when the particle size is close to the wavelength of light), and then begins to decrease. The effects of heat and pressure on two plant protein dispersions at different pH levels were investigated (Figure 2C D). Compared to the untreated samples, the turbidity of both SPI and MBP dispersions increased after heating. This indicates that temperature significantly affects the aggregation of SPI and MBP. Additionally, the extremely large particle size in the untreated protein dispersions may have caused their rapid settling. Therefore, these particles were not detected during the turbidity measurements because they had already settled at the bottom of the container before light passed through it. Notably, the highest turbidity was observed for both plant proteins at pH 5. This phenomenon may be due to the massive aggregation of proteins near the isoelectric point. When the pH is lower or higher than the isoelectric point of the protein, the turbidity decreases significantly because the electrostatic repulsion between protein molecules increases, inhibiting aggregation[46]. It is worth noting that turbidity significantly decreased ($p < 0.05$) as the pH increased from 7.0 to 11. This reduction in turbidity may be attributed to the strong electrostatic repulsion between SPI and MBP molecules under alkaline pH conditions during high-temperature and high-pressure processing, leading to the disruption of electrostatic-induced primary aggregates and weakened intermolecular aggregation.

View Article Online
DOI: 10.1039/D5FB00037A

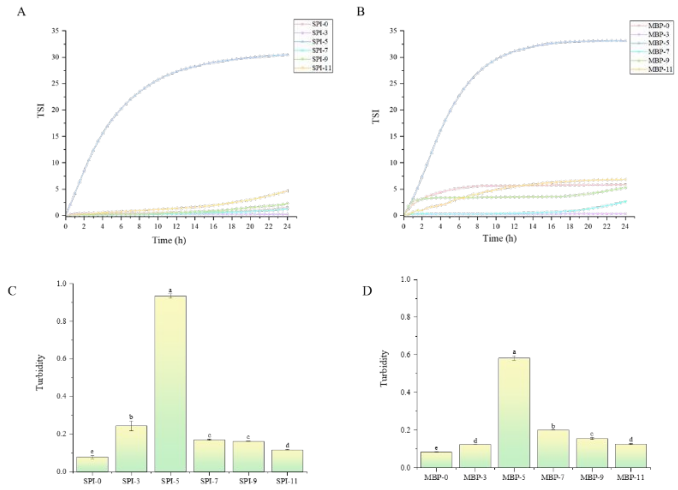

Figure 2 Effect of heat-pressing treatment at different pH values on the Turbiscan stability index (A, B) and turbidity (C, D) of soybean protein (SPI) and mung bean protein (MBP). SPI-0 and MBP-0 denote untreated samples, whereas the numbers following SPI and MBP (3, 5, 7, 9, and 11) indicate the pH values of the treated samples. Different letters above the bar charts indicate significant differences between groups ($p < 0.05$).

3.7 Surface hydrophobicity (H_0)

Surface hydrophobicity (H_0) is a critical determinant of protein surface properties[47]. This characteristic reflects alterations in the distribution of hydrophobic groups on the protein surface due to structural modifications. A common fluorescent probe, ANS, was employed to assess the surface hydrophobicity of proteins subjected to high-humidity heat treatment[48]. As illustrated in the (Figure 3A B), the H_0 values for SPI3 and MBP3 were 483.3 and 702.0, respectively. Acidic pH treatment resulted in an increase in H_0 values compared to the initial state, whereas alkaline pH treatment led to a decrease. Melt spheres are categorized into wet melt spheres (WMG) and dry melt spheres (DMG), with DMG unable to bind ANS in contrast to WMG[49]. Consequently, at pH 11, SPI11 and MBP11 exhibited values of 134.0 and 193.77, respectively. This trend is contrary to that observed in foaming ability. Elevated H_0 facilitates protein adsorption at the interface[50]. However, SPI-11 and MBP11, which demonstrated high foaming performance, exhibited the lowest hydrophobicity. Thus, the molecular mechanism underlying foaming is primarily linked to increased protein denaturation.

3.8 Surface tension

The surface activity of proteins significantly affects their capacity to adsorb at the gas-liquid interface and subsequently form foams[51]. By evaluating the impact of heat treatment high-pressure on surface activity across various pH levels for different protein dispersions, the time-dependent variation curves of their surface tension were ascertained (Figure 3 C D). Notably, the surface tension of all treated proteins was lower than that of the untreated proteins. This reduction may be attributed to the alteration in the size of colloidal particles within the protein dispersion subjected to heat treatment high-pressure, which modifies their surface chemical properties. Furthermore, the surface tension of plant proteins is influenced by the pH during treatment, with a decrease in the final value observed as the pH increases. At elevated pH levels, protein molecules may partially unfold due to enhanced electrostatic repulsion within the polypeptide chain, leading to the exposure of more nonpolar groups to the surrounding aqueous phase, thereby augmenting their ability to adhere to the gas-water interface[14]. Additionally, protein hydrolysis may occur under alkaline conditions, resulting in the formation of surface-active peptides that can adsorb onto the gas-water interface [52].

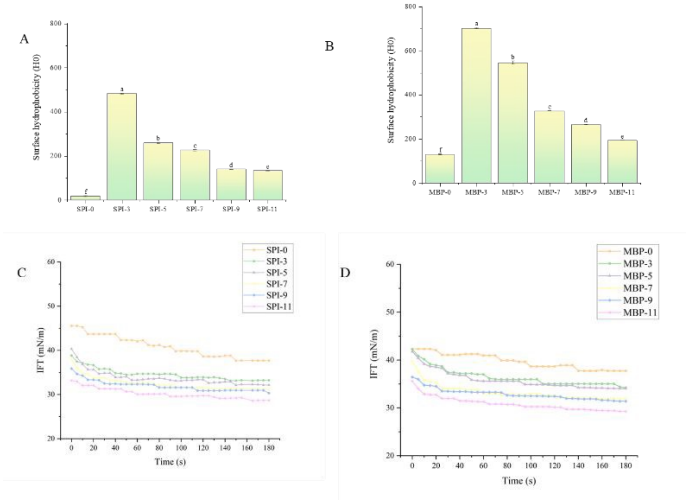

Figure 3 Effect of heat-press treatment at different pH values on the surface hydrophobicity (AB) and surface tension (CD) of soybean protein isolate (SPI) and mung bean protein (MBP). SPI-0 and MBP-0 denote untreated samples, whereas the numbers following SPI and MBP (3, 5, 7, 9, and 11) indicate the pH values of the treated samples. Different letters above the bar indicate significant differences between the groups ($p < 0.05$).

3.9 Foaming capacity and foam stability

The foaming properties of proteins reflect their flexibility and ability to adsorb at the gas-water interface, which is crucial for their application in foamed foods such as whipped cream and ice cream[53].The impact of heat treatment high-pressure at varying pH levels on the foaming performance of SPI and MBP is illustrated in Figure 4. The foaming activity (FA) of untreated SPI was 48.83%, while that of MBP was 102.0%. The foaming ability of both proteins was markedly enhanced following heat treatment high-pressure. Overall, as the pH increased from 3 to 11, the foaming ability of both proteins improved. The FA values of SPI-11 and MBP-11 were 120.66% and 130.66%, respectively. This suggests that extreme pH conditions significantly enhanced the foaming performance of SPI and MBP, potentially due to the partial unfolding of protein molecules under alkaline conditions, which leads to increased surface activity and the formation of molten globules with balanced amphiphilic properties and more flexible structural states[54]. These findings align with those of Zhao et al., who reported that the optimal foaming ability of milk proteins occurs at pH 11[55]. Additionally, pH shifts can reduce protein particle size. Smaller proteins are more readily adsorbed onto the air-water interface, resulting in superior foaming performance compared to larger proteins[56]. Furthermore, after heat treatment high-pressure, the foam stability of soy protein either remained similar to or slightly

View Article Online
DOI: 10.1039/D6FB00083A

decreased compared to that before treatment. For MBP, post-treatment foam stability exhibited only minor improvement, which was weakly correlated with pH. This effect may arise because the ability of protein particles to form protective coatings around bubbles does not strongly depend on their size or surface properties. It is speculated that all types of protein particles can form robust viscoelastic interface layers to stabilize bubbles[56].

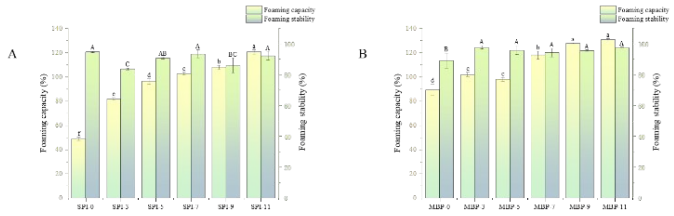

Figure 4 Effect of thermal pressure treatment at different pH values on the foaming capacity (A) and foaming stability (B) of soybean protein isolate (SPI) and mung bean protein (MBP). SPI-0 and MBP-0 denote untreated samples, whilst the numbers following SPI and MBP (3, 5, 7, 9 and 11) indicate the pH values of the treated samples. Different letters above the bar charts indicate significant differences between groups ($p < 0.05$).

3.10 Foam density, overrun, and porosity

The impact of high humidity and heat at different pH values on the foaming properties of the proteins was also assessed by measuring the foam density, overrun, and porosity (Table 2). All heat treatment high- pressure led to a substantial decrease in density, increase in overrun, and increase in the porosity of the foams formed by the two plant proteins. This suggests that these treatments increased the ability of the proteins to incorporate and stabilize air bubbles within the foam. The pH under high humidity and heat had an appreciable effect on the foaming properties of the proteins. For foams formed using both SPI and MBP, the density decreased, overrun increased, and porosity increased as the pH increased. This suggests that plant proteins have better foaming properties under alkaline conditions than under acidic conditions. As discussed earlier, this trend may have been due to the reduction in particle size and change in the surface chemistry of the proteins at higher pH values. Under strong alkaline conditions, the polypeptide chains would have partially unfolded, thereby exposing more non-polar groups at the protein surfaces, which could then attach to the air-water interface more easily[57]. Moreover, smaller protein particles could move to the air-water interface more rapidly during shearing, thereby producing smaller and more numerous air bubbles within the foams.

In general, the foaming properties of MBP were better than those of soybean proteins, as indicated by the higher overrun and porosity values. This effect may be attributed to the higher content of non-polar amino acids on the surface of MBP, which increased their surface hydrophobicity. In addition, the mung bean particles were smaller than the soy protein particles (Table 1), which may have facilitated their movement to the air-water interface during shearing.

Table 2. Impact of pH on foam density, overrun, and porosity of soy protein isolate (SPI) and mung bean protein (MBP).

Sample	SPI			MBP		
	Density (g/cm^3)	Overrun (%)	Porosity (%)	Density (g/cm^3)	Overrun (%)	Porosity (%)
0	0.69 ± 0.01^{a}	30.90 ± 2.50^{E}	$23.80\pm1.50^{e'}$	0.66 ± 0.02^{a}	21.90 ± 2.60^{D}	$18.0\pm1.80^{c'}$
3	0.48 ± 0.03^{b}	80.06 ± 0.74^{D}	$47.11\pm0.21^{d'}$	0.39 ± 0.01^{b}	129.10 ± 4.0^{C}	$56.34\pm0.78^{b'}$
5	0.45 ± 0.01^{c}	102.30 ± 1.80^{C}	$50.55\pm0.45^{c'}$	0.39 ± 0.01^{b}	131.10 ± 1.90^{BC}	$56.72\pm0.35^{b'}$
7	0.38 ± 0.01^{d}	134.90 ± 1.70^{B}	$57.43\pm0.30^{b'}$	0.37 ± 0.01^{b}	142.10 ± 6.20^{B}	$58.7\pm1.00^{b'}$
9	0.38 ± 0.01^{d}	137.60 ± 3.80^{B}	$57.91\pm0.67^{b'}$	0.37 ± 0.01^{b}	143.20 ± 4.00^{B}	$58.86\pm0.68^{b'}$
11	0.35 ± 0.01^{e}	159.10 ± 2.70^{A}	$61.41\pm0.40^{a'}$	0.34 ± 0.01^{c}	169.10 ± 9.00^{A}	$62.8\pm1.30^{a'}$

3.11 Foam microstructure

The microstructures of foams prepared by heat treatment high-pressure at different pH values were characterized using confocal fluorescence microscopy (Figure 5). The proteins were fluorescently labelled prior to observation to clearly determine their distribution and location within the foam structure. The microstructures of the foams were monitored at different time points. In addition, the overall morphological changes in the unlabelled foam bubbles were observed using a conventional optical microscope. The foaming activities (FA) and foaming stabilities (FS) of SPI and MBP were evaluated. The shape, particle size distribution, and density of foams are closely related to the foaming characteristics of proteins. Specifically, smaller bubbles tend to aggregate into more deformable structures, resulting in foams with higher drainage stability[58]. Initially, the foam contained uniformly distributed small bubbles after shearing; however, the bubble size increased over time, which was attributed to bubble coalescence and Ostwald ripening [59]. However, the rate and extent of bubble growth depend on the pH and protein type. Ideally, a good foaming agent should form small, uniformly distributed bubbles during shear, which should remain stable over time.

The foaming performances of the different protein samples differed significantly. For processed soy protein, the pH 5 sample exhibited protein aggregation between bubbles after long-term storage, which can be attributed to the isoelectric point precipitation effect. Interestingly, strongly alkaline soy protein samples (pH 9 and 11) exhibited a bimodal distribution of bubbles after long-term storage, with large and small bubbles alternating. After long-term storage, the bubble size in untreated soy protein samples appeared to be smaller than that in treated samples. This suggests that larger aggregates in untreated samples inhibit bubble coalescence or Ostwald ripening more effectively. These results are consistent with the foam stability results discussed in the previous section. For MBP, the initial and final bubble sizes of the untreated protein were larger than those of the treated protein, consistent with the previously discussed foaming capacity and foam stability results. For the treated MBP, the bubble distribution in the pH 5 samples appeared more uneven, primarily attributable to the isoelectric point precipitation of proteins in these systems. At pH 3, 7, 9, and 11, the bubble size increased during storage, and the increase was similar across all samples, consistent with the foaming ability and foam stability results. These results further indicate that pH changes significantly enhance the foaming properties of SPI and MBP, with optimal foaming performance at pH 11.

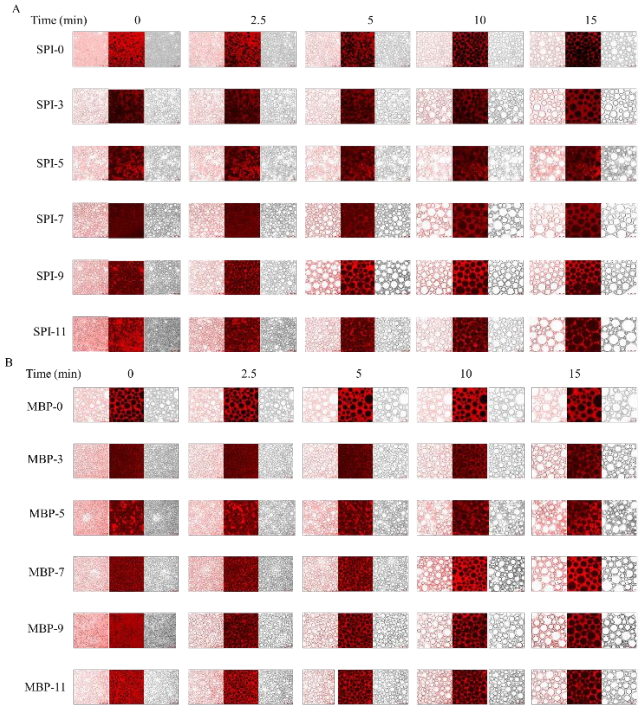

Figure 5 Confocal laser scanning microscopy (CLSM) images of stable foams of soybean protein isolate (SPI) and mung bean protein (MBP) following thermal compression treatment at different pH values. SPI-0 and MBP-0 denote untreated samples, whereas the numbers following SPI and MBP (3, 5, 7, 9, and 11) indicate the pH values at which the samples were treated.

Conclusions

This study investigated the effects of heat treatment high-pressure on the structure, physicochemical properties, and foaming performance of SPI and MBP under different pH conditions. The results indicated that heat treatment high-pressure at different pH levels significantly influenced the physicochemical properties, structure, and foaming performance of SPI and MBP. This treatment enhanced the foaming ability of both plant proteins, whereas the foam stability remained largely unaffected. In particular, under extreme alkaline conditions, changes in pH significantly improved the foaming performance of SPI and MBP. Under alkaline conditions, an increase in the negative charges on the peptide chains causes the protein molecules to become more flexible and unfold. The size of the protein particles decreased, and their surface properties changed, thereby altering their ability to form and stabilise foam. Specifically, these changes reduce the surface tension at the gas-liquid interface, potentially increasing the adsorption rate and enhancing the foaming ability of the proteins.

In summary, this study demonstrates that heat treatment high-pressure of protein solutions at different pH values can improve the foaming performance of plant-based proteins. Alkaline conditions exhibited superior foaming performance. These findings suggest potential food applications, such as alkaline beverages, whipped cream, and coffee cream, which require pH-dependent foaming performance, potentially enhancing their value as functional ingredients in the food industry. Future research could explore the effects of multi-factor synergistic interactions on the foaming performance and interfacial properties of plant proteins and apply these findings to novel food systems (e.g. plant-based meat products, artificial dairy products, and functional beverages) to investigate how foaming performance and interfacial properties influence product quality in these systems.

Author contributions

Xinyu Zhang: Experimental design, All the experiment conduction, Data analysis, Writing- Original draft preparation. **Tianlong Xiao**: Experimental design, All the experiment conduction, Data analysis, Writing- Original draft preparation. **David Julian McClements**: Experimental design, Writing - Review & Editing. **Hui Hu**: Investigation, Supervision. **Jinjin Zhu**: Investigation, Supervision. **Xiaojie Ma**: Methodology, Supervision, Funding acquisition. **Qiang Wang:** Conceptualization, Supervision, Funding acquisition. **Aimin Shi:** Methodology, Supervision, Funding acquisition.

Conflicts of interest

The authors declare no competing financial interests.

Data availability

All raw experimental data statistical data supporting the findings of this study are available from the corresponding author on reasonable request

Acknowledgements

This research was funded by the National Key Research and Development Program of China (2023YFE0104900), National Natural Science Foundation of China (32472271, 32172149) and Agricultural Science and Technology Innovation Project (CAAS-ASTIP-2025-IFST).

Notes and references

1. X. Zhang, Z. Liu, X. Ma, Y. Zheng, H. Hu, B. Jiao, D. J. McClements, Q. Wang and A. Shi, Food Chemistry, 2025, 463, 141431.
2. S.-Y. Tu, X.-Y. Hao, S. Xu, W. Liao, H. Xia, S.-K. Wang and G.-J. Sun, Food & Medicine Homology, 2026, 3, 9420136.
3. Z. Kang, S. Zhang, Y. Kong, Z. Wu, Y. Li, T. Liu and F. Xie, Food Structure, 2024, 42, 100383.
4. F. Speroni, M. de Lamballerie and M. Anton, Innovative Food Science & Emerging Technologies, 2024, 96, 103768.
5. R. Bai, Z. Li, L. Zhang, S. Jiang, J. Yu, A. Madina, X. Ye, C. Yang, Y. Chen, S. Wang and W. Ding, International Journal of Biological Macromolecules, 2024, 260, 129585.
6. M. Tarahi, L. Abdolalizadeh and S. Hedayati, Food Chemistry, 2024, 444, 138626.
7. G. Liang, W. Chen, K. Guo, Z. Wang, Q. Chen, M. Zeng, Z. He, H. D. Goff, T. Xin and J. Chen, Food Bioscience, 2025, 74, 107844.
8. L. L. Prates, M. E. Rodríguez Espinosa, X. Feng, M. Tosta, J. He and P. Yu, Animal Feed Science and Technology, 2023, 304, 115736.
9. X. Liu, K. Wei, Z. Wang, L. Jiang, J. Du, Z. Huang and T. Tian, Food Hydrocolloids, 2025, 168, 111538.
10. L. Scheuer, V. Mair, K. Hasenkopf, S. Bader-Mittermaier, U. Schweiggert-Weisz and S. Gola, Food Structure, 2026, 47, 100507.
11. J. Yan, S. Zhao, X. Xu and F. Liu, Current Research in Food Science, 2024, 8, 100653.
12. Y. Wang, S. Wang, R. Li, Y. Wang, Q. Xiang, K. Li and Y. Bai, Food Hydrocolloids, 2022, 124, 107351.
13. I. Othmeni, R. Karoui and C. Blecker, International Journal of Biological Macromolecules, 2024, 278, 134818.
14. X. Ma, M. Habibi and L. M. C. Sagis, Food Hydrocolloids, 2024, 155, 110228.
15. S. Wang, S. Miao and D.-W. Sun, Trends in Food Science & Technology, 2024, 143, 104285.
16. D. E. Igartúa, M. C. Dichano, S. B. Ferrari, G. G. Palazolo and D. M. Cabezas, Food Chemistry, 2024, 433, 137319.
17. F. Higa, C. Nickerson and M. T. Nickerson, Cereal Chemistry, 2025, 102, 89-101.
18. Y. Wang, F. Yang, M. Wu, J. Li, Y. Bai, W. Xu and S. Qiu, LWT, 2020, 131, 109812.
19. M.-P. Wang, X.-W. Chen, J. Guo, J. Yang, J.-M. Wang and X.-Q. Yang, Food Hydrocolloids, 2019, 87, 619-628.
20. W. Li, S. Faisal, X. Guo, S. Li, A. Shi, B. Jiao and Q. Wang, Food Chemistry, 2023, 426, 136615.
21. T. Li, J. Zhang, A. Hu, F. Guo, H. Zhou and Q. Wang, Food Hydrocolloids, 2024, 156, 110314.
22. C. Wu, Z. Liu, X. Hei, S. Li, B. Jiao, X. Ma, H. Hu, D. J. McClements, Q. Wang and A. Shi, Food Hydrocolloids, 2025, 160, 110833.
23. C. Wu, Z. Liu, L. Zhi, B. Jiao, H. Hu, X. Ma, J. Zhu, M. Pignitter, Q. Wang and A. Shi, Food Hydrocolloids, 2023, 144, 109012.
24. A. Hu, T. Li, H. Zhou, F. Guo, Q. Wang and J. Zhang, Food Hydrocolloids, 2024, 152, 109935.
25. X. Zhang, X. Ma, C. Wu, Y. Zheng, H. Hu, D. J. McClements, Q. Wang and A. Shi, International Journal of Biological Macromolecules, 2026, 354, 151311.
26. J. Dehghannya, M. Pourahmad, B. Ghanbarzadeh and H. Ghaffari, Journal of Food Engineering, 2018, 238, 164-177.
27. H. Wei, W. Wang, Z. Peng and J. Yang, Genomics, Proteomics & Bioinformatics, 2024, 22, qzae001.
28. M. Geng, L. Li, X. Feng, J. Xu, Y. Huang, F. Teng and Y. Li, Journal of Molecular Liquids, 2022, 360, 119511.
29. X. Du, M. Zhao, N. Pan, S. Wang, X. Xia and D. Zhang, Food Chemistry, 2021, 362, 130222.
30. X. Sun, S. He, Y. Ye, X. Cao, H. Liu, Z. Wu, J. Yue, R. Jin and H. Sun, Food Chemistry, 2020, 329, 127183.
31. F. Zaaboul, P. K. Borah and V. di Bari, Food Chemistry Advances, 2025, 6, 100943.
32. J. Jiang, J. Chen and Y. L. Xiong, Journal of Agricultural and Food Chemistry, 2009, 57, 7576-7583.
33. M. Yang, Y. Tang, N. Huang, S. Guo, J. Wu, Z. Li, Y. Sun, Y. Zhu and J. Ran, International Journal of Biological Macromolecules, 2025, 318, 145115.
34. J. Jiang, Q. Wang and Y. L. Xiong, Current Opinion in Food Science, 2018, 19, 50-56.
35. M. A. Malik, H. K. Sharma and C. S. Saini, Ultrasonics Sonochemistry, 2017, 39, 511-519.
36. S. Yang, L. Tao, Z. Yan, K. Ouyang, Q. Zhang, Y. Feng and Q. Zhao, Food Bioscience, 2025, 66, 106166.
37. O. E. Sponton, A. A. Perez, J. V. Ramel and L. G. Santiago, Food Hydrocolloids, 2018, 77, 863-869.
38. H. Dong, L. Yang, Y. Dadmohammadi, P. Li, T. Lin, Y. He, Y. Zhou, J. Li, G. Meletharayil, R. Kapoor and A. Abbaspourrad, Food Chemistry, 2024, 434, 137371.
39. N. Li and A. L. Girard, Food Hydrocolloids, 2023, 134, 108100.
40. Q. Zhao, L. Ding, M. Xia, X. Huang, K. Isobe, A. Handa and Z. Cai, Food Hydrocolloids, 2021, 120, 106876.
41. O. F. Eze, A. Chatzifragkou and D. Charalampopoulos, Food Chemistry, 2022, 368, 130837.
42. X. Hu, Q. Ju, C. K. W. Koo and D. J. McClements, Food Hydrocolloids, 2024, 147, 109333.
43. Z. Liu, A. Shi, C. Wu, X. Hei, S. Li, H. Liu, B. Jiao, B. Adhikari and Q. Wang, ACS Applied Materials & Interfaces, 2022, 14, 57350-57361.
44. Q. Mu, H. Su, Q. Zhou, S. Xiao, L. Zhu, X. Xu, S. Pan and H. Hu, Food Chemistry, 2022, 381, 132158.
45. R. Zhao, W. Fu, D. Li, C. Dong, Z. Bao and C. Wang, Journal of Dairy Science, 2024, 107, 726-741.
46. Q. T. Zhang, Z. C. Tu, H. Wang, X. Q. Huang, L. L. Fan, Z. Y. Bao and H. Xiao, J Food Sci Technol, 2015, 52, 3412-3421.
47. X. Hei, S. Li, Z. Liu, C. Wu, X. Ma, B. Jiao, H. Hu, J. Zhu, B. Adhikari, Q. Wang and A. Shi, Food Chemistry, 2024, 449, 139187.
48. T. Xiao, X. Ma, H. Hu, F. Xiang, X. Zhang, Y. Zheng, H. Dong, B. Adhikari, Q. Wang and A. Shi, Food Chemistry: X, 2025, 29, 102792.
49. T. Zhang, T. Chen, H. Jiang, J. Liu, E. Wang, M. Zhang and X. Liu, Food Hydrocolloids, 2023, 144, 109060.

View Article Online
DOI: 10.1039/D6FB00023A

50. M. Li, M. Li, W. Tan, X. Liu and X. Duan, Journal of Food Engineering, 2019, 261, 158-164.
51. X. Zhang, Q. Wang, Z. Liu, L. Zhi, B. Jiao, H. Hu, X. Ma, D. Agyei and A. Shi, Food Hydrocolloids, 2023, 144, 109008.
52. P. Bertsch, L. Böcker, A.-S. Palm, J. Bergfreund, P. Fischer and A. Mathys, Food Hydrocolloids, 2023, 136, 108290.
53. Z. Li, X. Huang, J. Guo, Y. Hu, K. Gafurov, J. Zhang, Q. Wang and Q. Guo, Food Hydrocolloids, 2026, 172, 112017.
54. L. Wang, J. Wen, L. Wang, L. Jiang, Y. Zhang and X. Sui, Food Hydrocolloids, 2023, 144, 109040.
55. X. Zhao, X. Fan, X. Shao, M. Cheng, C. Wang, H. Jiang, X. Zhang and C. Yuan, Ultrasonics Sonochemistry, 2022, 88, 106089.
56. S. Jiang, J. Ding, J. Andrade, T. M. Rababah, A. Almajwal, M. M. Abulmeaty and H. Feng, Ultrasonics Sonochemistry, 2017, 38, 835-842.
57. S. Momen, F. Alavi and M. Aider, Trends in Food Science & Technology, 2021, 110, 778-797.
58. Q. Wang, Y. Jin and Y. L. Xiong, Journal of Agricultural and Food Chemistry, 2018, 66, 10827-10834.
59. M. Assad Bustillos, C. Jonchère, C. Garnier, A. L. Réguerre and G. Della Valle, Food Hydrocolloids, 2020, 101, 105553.

View Article Online
DOI: 10.1039/D6FB00023A

Data Statement: All raw experimental data statistical data supporting the findings of this study are available from the corresponding author on reasonable request.